PTEP

Prog. Theor. Exp. Phys. **2021**, 103D02 (11 pages)
DOI: 10.1093/ptep/ptab087

Deformation effect on nuclear density profile and radius enhancement in light- and medium-mass neutron-rich nuclei

Wataru Horiuchi[1,*] and Tsunenori Inakura[2]

[1]*Department of Physics, Hokkaido University, Sapporo 060-0810, Japan*
[2]*Laboratory for Advanced Nuclear Energy, Institute of Innovative Research, Tokyo Institute of Technology, Tokyo 152-8550, Japan*
*E-mail: whoriuchi@nucl.sci.hokudai.ac.jp

Received March 31, 2021; Revised June 25, 2021; Accepted June 25, 2021; Published July 14, 2021

The mass number dependence of nuclear radii is closely related to the properties of nuclear matter. It is known that most nuclei exhibit some deformation. We discuss how the nuclear density profile is modified by nuclear deformation to elucidate the enhancement mechanism of nuclear radii through a systematic investigation of neutron-rich Ne, Mg, Si, S, Ar, Ti, Cr, and Fe isotopes. Skyrme–Hartree–Fock calculations are performed in a 3D Cartesian grid to describe the nuclear deformation in a non-empirical way. The role of nuclear deformation in nuclear density profiles is explored in comparison to calculations with a spherical limit. We find correlations between nuclear deformation and the internal nuclear density. The evolution of nuclear radii appears to follow the core swelling mechanism recently proposed in spherical nuclei [W. Horiuchi and T. Inakura, Phys. Rev. C **101**, 061301(R) (2020)], and the radius is further enhanced by nuclear deformation. This study demands further theoretical and experimental investigations for the internal density.

Subject Index D04, D12, D13

1. Introduction

The nuclear landscape has been extended toward the neutron dripline and has so far reached the Ne isotopes [1]. Following the discovery of new neutron-rich isotopes, the evolution of nuclear radii in terms of the neutron excess is of interest as it is closely related to the properties of "matter" composed of neutrons and protons in particularly extreme neutron/proton ratios [2–7].

For stable nuclei, the mass number (A) dependence of the nuclear matter radius is roughly proportional to $A^{1/3}$ due to the saturation of the nuclear density [8,9]. For neutron-rich unstable nuclei, many examples that deviate from this rule have been observed because of exotic structure properties, e.g., halo structure [10,12] (see also Ref. [11] and references therein) and nuclear deformation [13,14]. Approaching the neutron dripline, the emergence of deformed halo structure was predicted in Ne and Mg isotopes [15–20] and has actually been observed for ^{31}Ne [21].

Recently, indications of the "core" swelling in neutron-rich Ca isotopes have been reported [22,23], exhibiting a kink in the charge and matter radii at $N = 28$. In Ref. [24], this phenomenon was related to the nuclear internal density in that the "core" density swells to reduce the internal density to increase the total energy. We remark that another mechanism to produce a kink in the charge radius for heavy nuclei was proposed in Ref. [25]. Since most nuclei are deformed [26], it is natural to extend the study of Ref. [24] to deformed neutron-rich nuclei.

The purpose of this paper is to clarify the radius enhancement mechanism of neutron-rich unstable nuclei, focusing on the role of nuclear deformation. We study light- and medium-mass nuclei with the proton number $8 < Z < 28$, where their isotope dependence is significant. It is well known that nuclear deformation considerably enhances the matter radius in the light-mass neutron-rich isotopes Ne and Mg [13,14,27–31]. We investigate how the density profiles are changed by nuclear deformation and discuss its correlation with the internal density. Skyrme–Hartree–Fock (HF) calculations in 3D Cartesian coordinates are performed, which allow us to describe any deformed shape. Since the nuclear deformations predicted are strongly model dependent, several sets of standard Skyrme-type effective interactions are investigated.

The paper is organized as follows. Section 2 introduces the theoretical model employed in this paper. Model setups of the HF calculation to obtain the deformable ground-state wave functions are briefly explained. Section 3 is devoted to a discussion of changes in the density profiles and the enhancement mechanism of the nuclear radius due to nuclear deformation based on the HF results. We compare these results with spherically constrained HF to clarify the role of the nuclear deformation. Section 3.1 discusses the evolution of nuclear deformation as a function of the neutron number for neutron-rich isotopes with $8 < Z < 28$. Section 3.2 describes the deformation effect on the density profiles. We compare the density distributions obtained with full and spherically constrained HF calculations for some selected nuclei, ^{34}Mg, ^{40}S, and ^{62}Cr. The role of nucleon orbits near the Fermi level is quantified. Section 3.3 contains more general discussions that relate nuclear deformation and nuclear density in the internal region. Finally, the conclusion is given in Sect. 4.

2. Skyrme–Hartree–Fock calculation in 3D coordinate space

In this paper, we employ the Skyrme–HF calculation. Since all details can be found in Refs. [24,30,32], we only give a minimum explanation for the present analysis. The ground-state wave function is expressed as a product of deformable single-particle (s.p.) orbits represented by a 3D Cartesian mesh that is flexible enough to describe any nuclear deformation. We obtain these s.p. orbits fully self-consistently in a sphere of radius 20 fm based on the energy density functional of the intrinsic nucleon density $\tilde{\rho}$ [33], $E[\tilde{\rho}] = E_N + E_C - E_{\rm cm}$, where E_N is the nuclear energy, E_C the Coulomb energy, and $E_{\rm cm}$ the center-of-mass energy. The total energy is minimized using the imaginary-time method [34]. The Coulomb interaction is incorporated as given in Ref. [35]. This paper aims to understand the nuclear deformation effect on the density profile, which is an extension of the previous study for spherical nuclei [24]. To obtain different density profiles, four kinds of Skyrme parameter sets, SkM* [36], SLy4 [37], SkI3 [38], and SIII [39] are employed. As a reference to clarify the role of nuclear deformation, we also perform a spherically constrained HF calculation. To preserve the spherical symmetry, the self-consistent HF solution is obtained with the filling approximation [39], which assumes a uniform occupation of the Fermi level with angular momentum j as $m/(2j+1)$ with m being the number of outermost nucleons. We remark that the pairing correlation is an important ingredient for determining the nuclear deformation. However, at this stage, the pairing correlation is ignored because it may induce further model dependence; see, e.g., Refs. [26,40–43].

To guide the degree of nuclear deformation, the quadrupole deformation parameter of the ground-state wave function is evaluated; this is defined by

$$\beta_2 = \sqrt{\beta_{20}^2 + \beta_{22}^2}, \tag{1}$$

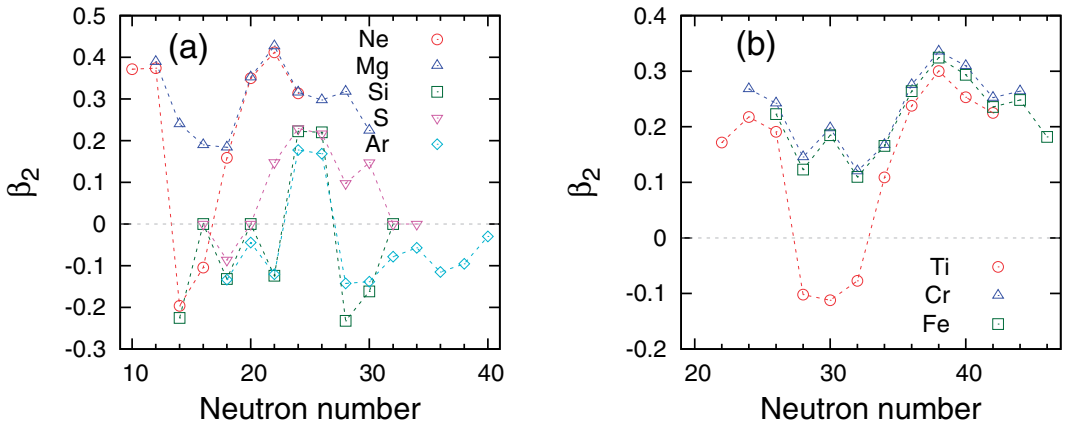

Fig. 1. Quadrupole deformation parameter of (a) Ne, Mg, Si, S, and Ar and (b) Ti, Cr, and Fe isotopes as a function of the neutron number. The SkM* interaction is employed.

where

$$\beta_{20} = \sqrt{\frac{\pi}{5}}\frac{\langle 2z^2 - x^2 - y^2\rangle}{\langle r^2\rangle}, \quad \beta_{22} = \sqrt{\frac{3\pi}{5}}\frac{\langle y^2 - x^2\rangle}{\langle r^2\rangle} \tag{2}$$

with $r^2 = x^2 + y^2 + z^2$. We take z as the quantization axis and choose it as the largest (smallest) principal axis for prolate (oblate) deformation. Thus, the sign of β_2 follows that of β_{20}. The ground-state wave function can be triaxially deformed ($0 < \gamma < \pi/3$), which is treated as prolate ($0 < \gamma < \pi/6$) or oblate ($\pi/6 < \gamma < \pi/3$) for simplicity.

3. Results and discussions

3.1. Evolution of nuclear deformation

First we give an overview of the neutron number dependence of even–even neutron-rich isotopes with $8 < Z < 28$. Among the four Skyrme-type interactions employed in this paper, the SkM* interaction is best for describing the nuclear deformation and the validity of these density distributions for Ne and Mg isotopes were well evaluated as they showed good agreement with the measured cross sections [30,44]. It is the results obtained with the SkM* interaction that are mainly discussed, unless otherwise mentioned.

Figure 1 plots the quadrupole deformation parameter β_2 for those isotopes with (a) $8 < Z < 20$ and (b) $20 < Z < 28$ as a function of the neutron number. Let us first discuss the isotope dependence of the nuclear deformation for $8 < Z < 20$. The reader is referred to Ref. [30] for more discussions on the structure of those isotopes with $Z = 10$–14. Actually, the nuclear deformation strongly depends on the proton and neutron numbers. The proton and neutron numbers of $Z, N = 10$ and 12 favor a prolately deformed state due to the occupation of the $[nn_z m_l]\tilde{\Omega} = [220]1/2$ and $[211]3/2$ orbits, where n, n_z, m_l, and $\tilde{\Omega}$ denote the asymptotic quantum numbers [45]: the principal quantum number, that for the quantization axis z, the projection of the orbital angular momentum onto z, and that of the total angular momentum onto z, respectively. It is well known that Ne and Mg show large deformation in the island of inversion [14,46–49]. Most of the Ne and Mg isotopes show a prolate shape, whereas ^{24,26}Ne are oblately deformed.

To see the calculated results, the proton number of $Z = 14$ favors both the prolate and oblate states as the s.p. energy of the $[202]5/2$ orbit may compete with the prolately deformed orbits, e.g.,

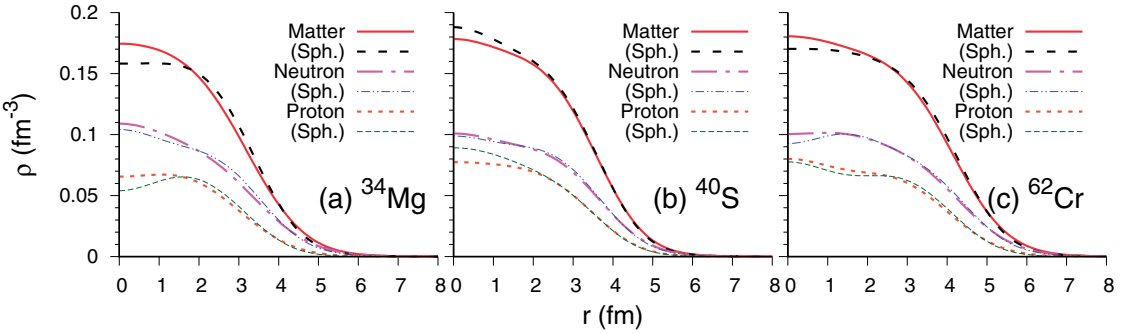

Fig. 2. Matter, neutron, and proton density distributions of (a) ^{34}Mg, (b) ^{40}S, and (c) ^{62}Cr obtained from the full and spherical (Sph.) HF calculations. The SkM* interaction is employed.

[220]1/2 and [211]3/2. Competing with changes in the neutron shell structure by neutron excess, Si isotopes have relatively small deformations $|\beta_2| \lesssim 0.2$. The proton number of $Z = 16$ favors a spherical shape, and thus S isotopes have small β_2 values like Si isotopes. Most of the Ar isotopes ($Z = 18$) exhibit oblate deformation. The nucleon number just before shell closure favors the oblate shape.

Figure 1(b) shows β_2 for the Ti, Cr, and Fe isotopes. Most medium-mass nuclei have a prolate shape; this is known as prolate dominance [50–52]. Oblate deformations are found only in $^{50-54}$Ti. ^{50}Ti forms an oblate shape that could be produced in the prolately deformed state from a combination of a subshell closed neutron orbit ($N = 28$) and a prolate-favoring [330]1/2 orbit ($Z = 22$). The Ti, Cr, and Fe isotopes have large deformations at $N \approx 38$, where additional occupancy of the [440]1/2 and [411]3/2 orbits is induced like in the island of inversion found at $N \approx 20$.

3.2. *Deformation effect on nuclear density profile*

In this subsection, we show some specific examples of how the density profile is modified by nuclear deformation. Figure 2 displays the point-matter, neutron, and proton density distributions of (a) ^{34}Mg, (b) ^{40}S, and (c) ^{62}Cr, which show the largest quadrupole deformation parameters for each isotope with the SkM* interaction. The deformed intrinsic density distributions are averaged over angles as $\rho(r) = \frac{1}{4\pi}\int d\Omega\, \tilde{\rho}(r,\Omega)$. The density distributions with the spherically constrained HF are also plotted for comparison. Compared to the spherical one, for the ^{34}Mg and ^{62}Cr cases, the deformed state shows a more diffused nuclear surface and higher internal density, like to the case of ^{30}Ne [30], whereas for ^{40}S the internal density is reduced by the nuclear deformation.

These changes in the density profile crucially affect the total energy, which can be quantified by showing the cumulative energy per nucleon defined by

$$\varepsilon(r) = \int_0^r r'^2 dr' \int d\Omega\, E[\tilde{\rho}(r',\Omega)] \Big/ \int_0^r r'^2 dr' \int d\Omega\, \tilde{\rho}(r',\Omega). \tag{3}$$

Note that $\varepsilon(r)$ with $r \to \infty$ leads to the energy per nucleon $E[\tilde{\rho}]/A$. Figure 3 displays $\varepsilon(r)$ of the full and spherically constrained HF of (a) ^{34}Mg, (b) ^{40}S, and (c) ^{62}Cr. Significant contributions of the internal density, say below $\approx$ 2–3 fm, can clearly be seen in the cumulative energies. The deformed nuclear states for ^{34}Mg and ^{62}Cr are more advantageous for energy gain than the spherical nuclear states, while the opposite is true in ^{40}S, where the nuclear internal density is reduced by nuclear deformation. It should be noted that deformed nuclear states always gain more energy than spherical ones in surface regions beyond $\approx$ 3–4 fm. The deformed state is selected in ^{40}S because

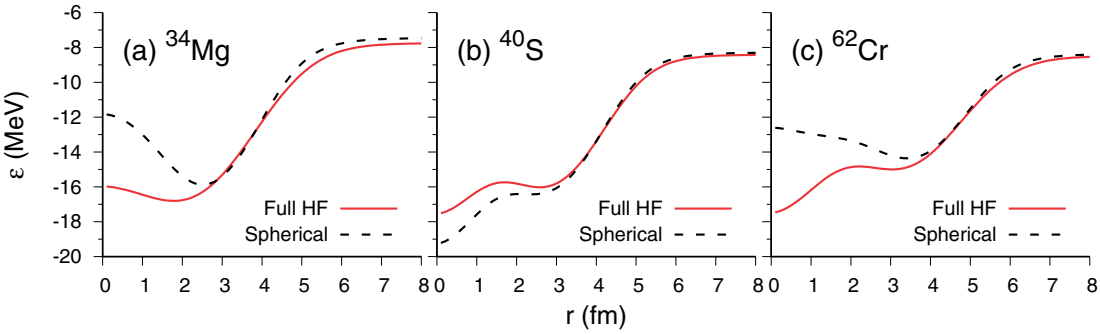

Fig. 3. Cumulative energies per nucleon of (a) ^{34}Mg, (b) ^{40}S, and (c) ^{62}Cr obtained from the full and spherically constrained HF calculations. The SkM* interaction is employed.

the energy gain in the surface region is larger than the energy loss in the internal region compared to the spherical state.

Since the characteristics of occupied s.p. orbits are crucial to determine the nuclear density distributions, we calculate the occupation probability of the spherical s.p. orbits for these deformed states. In practice, we simply take the overlap between the s.p. orbits of the full and spherical HF calculations. With this procedure, the components of the spherical s.p. orbits are projected out from each deformed s.p. orbit. The occupation probabilities for each spherical s.p. state are obtained by dividing those occupation numbers by the maximum occupation number $2j + 1$ for each s.p. state with the angular momentum j. Figure 4 displays these obtained occupation probabilities for the neutrons and protons of (a) ^{34}Mg, (b) ^{40}S, and (c) ^{62}Cr. The results with the spherical limit are also shown for comparison. The labels of the s.p. orbits are aligned in order of s.p. energy. We see that the nuclear deformation only affects the distribution around the Fermi levels, which makes the surface more diffuse due to the mixture of lower orbital-angular-momentum s.p. states, resulting in a further increase in the nuclear radius compared to the spherical limit. Regarding these fully occupied orbitals as belonging to the "core" of the nucleus, the structure change by nuclear deformation is governed by the "valence" nucleons.

Let us discuss this in more detail. In (a) ^{34}Mg, since the $1s_{1/2}$ orbit is located just above the proton Fermi level $0d_{5/2}$, the nuclear deformation induces occupancy of the $1s_{1/2}$ orbit, which leads to the enhancement of the central density as well as the nuclear diffuseness as seen in Fig. 2(a). The same phenomenon is also found in the case of $N = 14$ isotones [53]. The nuclear deformation induces occupancy of the $1s_{1/2}$ orbit and thus the central depression of the nuclear density disappears.

In contrast, in the case of (b) ^{40}S, the $1s_{1/2}$ orbit is fully occupied in the spherical limit. To get a deformed state, as the Fermi level for protons is $1s_{1/2}$, some of these protons should be moved to the other orbits around the Fermi level, i.e., the $0d_{3/2}$ orbit, resulting in the reduction of $1s_{1/2}$ occupancy, i.e., reduction of the central density compared to the spherical limit displayed in Fig. 2(b).

For ^{62}Cr, the mechanism is not simple as those for ^{34}Mg and ^{40}S because there is no vacant or occupied s orbit near the Fermi level for either protons or neutrons. Actually, the nuclear deformation induces a slight increase in the occupancy of the $2s_{1/2}$ orbit for neutrons. However, this is not enough to explain the enhancement of the central density presented in Fig. 2(c). What induces this enhancement of the central density? To understand this, we compare the central densities that come from the deepest s.p. orbits [000]1/2 and $0s_{1/2}$ obtained by deformed and spherical HF calculations, respectively. Since the full HF calculation produces a deeper mean-field potential than the spherical

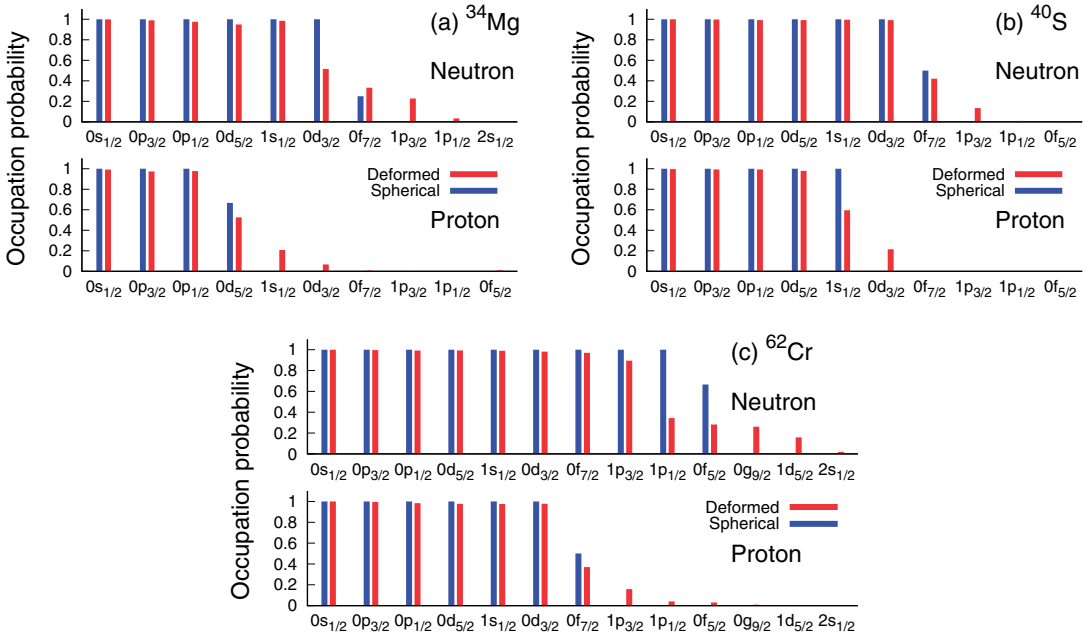

Fig. 4. Occupation probabilities of the full and spherically constrained HF single-particle (s.p.) orbits for (a) ^{34}Mg, (b) ^{40}S, and (c) ^{62}Cr. See text for details. The SkM* interaction is employed.

one, the $[000]1/2$ orbit is confined in a narrower potential well than that of the spherical $0s_{1/2}$ orbit. In fact, the respective s.p. energies are -44.41 and -43.29 MeV. The resulting central density of the $[000]1/2$ orbit for neutrons becomes approximately 10% higher than the spherical $0s_{1/2}$ orbit, which corresponds to about half of the total enhancement of the central density. This enhancement of the central density for protons is tiny, $\approx 1\%$. The other contribution may come from the change in the $1s_{1/2}$ orbit by the deformation, which is not easily identified as it is constructed from various deformed s.p. orbits.

We note that the pairing correlations also give fractional occupation probabilities for states around the Fermi level. Incorporating the pairing interaction is necessary for more quantitative discussions that involve close comparison with experimental data; see, e.g., Ref. [54] for Cr isotopes; however, this is beyond the scope of this paper.

3.3. Correlations of the nuclear deformation and internal density

In the previous subsection, we showed the energy contributions of the internal and surface density, which can be the trigger for nuclear deformation. Extending the discussion to more general cases, we evaluate the correlations between nuclear deformation and internal density. Here we take the central density $\rho(0) = \tilde{\rho}(0)$ as the degree of internal density for all isotopes studied in this paper.

Figure 5(a) displays a correlation plot of the relative differences in the central densities calculated by the full and spherically constrained HF calculations, $\Delta[\rho(0)] = [\rho(0) - \rho^{\text{sph.}}(0)]/\rho^{\text{sph.}}(0)$, with the SkM* interaction. We find that the $|\Delta[\rho(0)]|$ value becomes large for greatly deformed states. This indicates that the nuclear deformation can be driven by those changes in the internal density. Most of the isotopes are deformed by filling the internal densities, while most of the S and the Ar isotopes lower their internal densities by nuclear deformation. The most striking difference in these

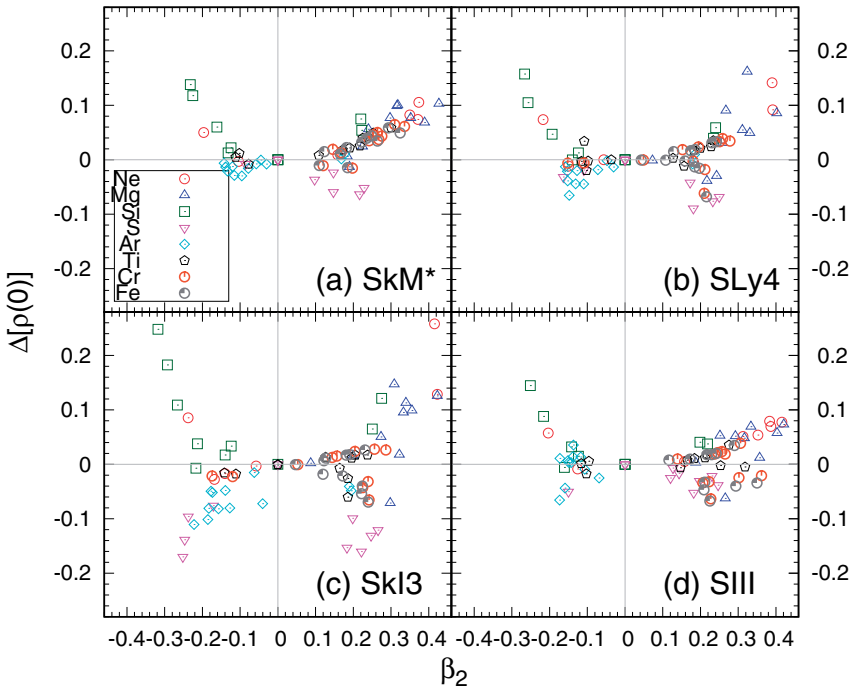

Fig. 5. Correlation plot of the relative differences in the central densities between the full and spherically constrained HF calculations versus the quadrupole deformation parameter β_2 of the Ne, Mg, Si, S, Ar, Ti, Cr, and Fe isotopes. The (a) SkM*, (b) SLy4, (c) SkI3, and (d) SIII interactions are employed.

isotopes compared to the others is that the central densities are quite high ≈ 0.18–0.19 fm^{-3} in the spherical limit because the $1s_{1/2}$ orbits are fully occupied, like in the case of ^{40}S [Fig. 2(b)].

We do the same analysis with the other Skyrme interactions, SLy4, SkI3, and SIII. The results are respectively displayed in Figs. 5(b), (c), and (d). Though there are some quantitative differences, a similar trend is obtained for the different Skyrme interactions. The larger $|\Delta[\rho(0)]|$ is, the larger $|\beta_2|$ becomes. The functional form of $|\Delta[\rho(0)]|$ appears to be a quadratic function of β_2. To quantify this correlation, we calculate the correlation coefficient of β_2^2 and $|\Delta[\rho(0)]|$ for each interaction. In fact, they show correlations as the calculated correlation coefficients are 0.77, 0.73, 0.66, and 0.54 for the SkM*, SLy4, SkI3, and SIII interactions, respectively. This square proportionality can roughly be explained within an assumption of volume conservation with a sharp radius R. Using the familiar radius formula $R' = R\sqrt{1 + (5/4\pi)\beta_2^2}$ [9] for a quadrupole deformed surface for small β_2, we get $\Delta[\rho(0)] \approx -\frac{15}{8\pi}\beta_2^2$. Though the estimation always predicts a negative value for $\Delta[\rho(0)]$, it gives $\Delta[\rho(0)] \approx -0.01$ to -0.05 for $|\beta_2| = 0.1$–0.3, which is reasonable. In reality, most of the cases show a positive $\Delta[\rho(0)]$ value owing to the modification of the surface distributions demonstrated in Figs. 2(a) and (c). This rough estimation can only be applied to the cases that exhibit relatively small changes in the surface density distributions, e.g., ^{40}S in Fig. 2(b).

Comparing the results with different Skyrme interactions, the behavior of $\Delta[\rho(0)]$ with the SkM* and SLy4 interactions is similar; the largest $\Delta[\rho(0)]$ values are shown with the SkI3 interaction, and the SIII interaction tends to give smaller values and the correlation becomes small. This fact may be related to the nuclear equation of state (EOS) parameters, which characterize the softness of the nuclear matter against nucleon excess. Some relevant values for each interaction are listed in Table 1. The listed EOS parameters are similar for the SkM* and SLy4 interactions. The SkI3 interaction

Table 1. Saturation density, incompressibility, symmetry energy, and the slope parameter of the symmetry energy for the adopted Skyrme interactions. Energy is given in MeV.

	ρ_0 (fm^{-3})	K_0	$E_{\rm sym}$	L
SkM*	0.1602	216.40	30.04	45.80
SLy4	0.1595	229.90	32.00	45.94
SkI3	0.1577	257.96	34.83	100.49
SIII	0.1453	355.35	28.16	9.91

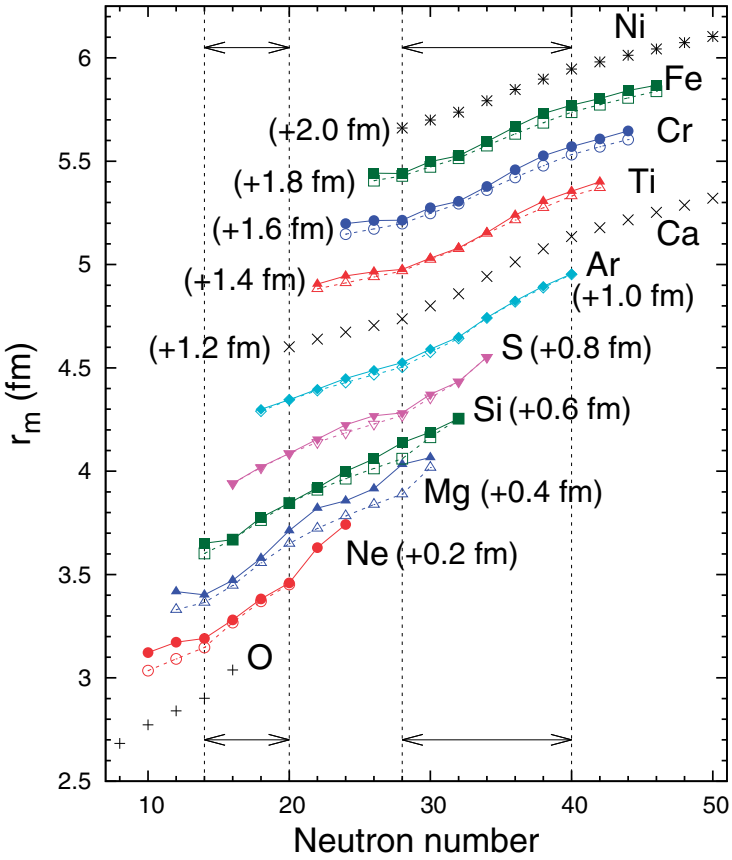

Fig. 6. Root-mean-square matter radii of O, Ne, Mg, Si, S, Ar, Ca, Ti, Cr, Fe, and Ni isotopes as a function of the neutron number. The open symbols denote the matter radii obtained with the spherically constrained HF calculations. The results of O, Ca, Ni are taken from Ref. [24]. For the sake of visibility, $(Z-8)\times 0.1$ fm is added to the results. Two-headed arrows indicate regions where core swelling is expected to occur. See text for more details. The SkM* interaction is employed.

has a very large slope parameter of the symmetry energy L, while the incompressibility K_0 and the symmetry energy $E_{\rm sym}$ are not very different from those for the SkM* and SLy4 interactions. Since the energy loss against the neutron and proton number asymmetry from the nuclear saturation density, i.e., 0.16 fm^{-3} for $N=Z$, is largest for the SkI3 interaction, a larger central density fraction $\Delta[\rho(0)]$ is needed to induce large nuclear deformation compared to the other interactions. In contrast, the SIII interaction gives extremely small L and large K_0. As displayed in Fig. 5, the $\Delta[\rho(0)]$ values are hard to change compared to the other interactions.

3.4. Evolution of the nuclear radius

How does nuclear deformation affect the nuclear radius? Figure 6 displays the root-mean-square (rms) matter radii r_m of those isotopes with $Z = 8$–28 calculated with full (closed symbols) and spherically constrained HF (open symbols) calculations. Note that we omit the results with the spherical HF calculations for ^{32,34}Ne because they are not bound. A kink in the nuclear radius across $N = 18$–20 for the Ne and Mg isotopes appears when the nuclear state exhibits large quadrupole deformation. The enhancement of the Ne isotopes near the dripline $N = 20$–24 is an exception that can be recognized as the systems have weakly bound orbits $\lesssim 3$ MeV. This is consistent with the findings of the systematic analyses given in Refs. [27–31,44].

We note that in the spherically constrained HF calculation, despite all the nuclear states being spherical, the matter radii already show some kinks at the magic and semi-magic numbers, i.e., $N = 14$, 20, and 28. This can be explained by the core swelling mechanism recently proposed in Ref. [24]. The enhancement of nuclear radii occurs when the valence neutrons fill the nodal or j-lower orbits, resulting in core swelling or enhancement of the nuclear radius to avoid high density in internal regions. For the sake of comparison, the results of the O, Ca, and Ni isotopes taken from Ref. [24] are shown. Their neutron number dependence is similar to those of the spherically constrained HF calculations from the Ne to Fe isotopes studied in this paper: A sudden enhancement of the nuclear radius occurs in the spherically constrained HF calculations for $N = 14$–20 when $1s_{1/2}$, $0d_{3/2}$ are occupied, and for $N = 28$–40 when $1p_{3/2}$, $0f_{5/2}$, and $1p_{1/2}$ are occupied.

We see that the deformed HF results always give larger radii than the spherical ones for all the isotopes studied in this paper. It is natural to presume that the radius enhancement occurs via the core swelling mechanism [24] and the radius is further enhanced when the nucleus exhibits nuclear deformation.

4. Conclusions

In order to elucidate the enhancement mechanism for nuclear radii, we have studied the effect of nuclear deformation on nuclear density profiles. A systematic investigation for even–even light- and medium-mass neutron-rich nuclei of $8 < Z < 28$ has been undertaken based on the ground-state density distributions obtained from Skyrme–Hartree–Fock calculations in a 3D Cartesian mesh. A spherically constrained HF calculation has also been performed as a reference state for each deformed HF state.

The nuclear internal density can be the key to understanding deformation phenomena. We have shown that nuclear deformation is determined by minimizing the total energy in the whole nuclear region, not only in the surface region but also in the internal region. We find correlations between changes in the internal density and nuclear deformation, which can be related to the properties of nuclear matter. A deformed nuclear state is selected to weigh the relative energy gains in the internal and surface regions. In general, the nuclear deformation induces a more diffuse nuclear surface while changing the magnitude of the density distributions in the internal regions. From a microscopic point of view, this phenomenon can be explained by considering the fact that the nuclear deformation mainly influences the occupation of spherical single-particle orbits near the Fermi level. Changes in the nuclear density in the internal regions become significant when the occupied or unoccupied s orbital is located near the Fermi level because its occupation number is strongly modified by nuclear deformation.

We have found that in the spherical limit the evolution of the nuclear radius with respect to the neutron number follows the core swelling rule proposed in Ref. [24], that a "core" nucleus swells when the single-particle orbits that have large spatial overlaps between the orbitals in the core. Core swelling is responsible for developing the nuclear bulk and nuclear deformation plays a role in diffusing the density profile in the surface regions, resulting in a further increase in the nuclear radius. The nuclear deformation mainly changes the occupation number near the Fermi level, while the occupation numbers of the deeper bound orbitals are not changed; even single-particle states are deformed. This is strong evidence that the core swelling phenomena found in spherical nuclei [23,24] is universal for radius enhancement, although the occupation number of single-particle orbits near the Fermi level becomes fractional by surface phenomena such as nuclear deformation.

In this paper, we have discussed possible correlations between nuclear deformation and internal density. We note, however, that this work only includes the deformation effect on the density profile with a standard mean-field approximation. To establish the results of this work, a careful investigation is necessary, including the pairing correlation and various many-body effects beyond the mean-field level. Also, experimental studies to extract the internal density of unstable nuclei are desired, such as electron scattering, which has recently been realized [55].

Acknowledgements

This work was in part supported by a Japan Society for the Promotion of Science (JSPS) KAKENHI Grant No. 18K03635. We acknowledge the collaborative research programme of 2021, Information Initiative Center, Hokkaido University.

References

[1] D. S. Ahn et al., Phys. Rev. Lett. **123**, 212501 (2019).
[2] L.-W. Chen, C. M. Ko, B.-A. Li, and J. Xu, Phys. Rev. C **82**, 024321 (2010).
[3] P.-G. Reinhard and W. Nazarewicz, Phys. Rev. C **81**, 051303(R) (2010).
[4] X. Roca-Maza, M. Centelles, X. Viñas, and M. Warda, Phys. Rev. Lett. **106**, 252501 (2011).
[5] M. Kortelainen, J. Erler, W. Nazarewicz, N. Birge, Y. Gao, and E. Olsen, Phys. Rev. C **88**, 031305(R) (2013).
[6] T. Inakura, T. Nakatsukasa, and K. Yabana, Phys. Rev. C **88**, 051305(R) (2013).
[7] X. Roca-Maza, X. Viñas, M. Centelles, B. K. Agrawal, G. Coló, N. Paar, J. Piekarewicz, and D. Vretenar, Phys. Rev. C **92**, 064304 (2015).
[8] H. de Vries, C. W. de Jager, and C. de Vries, At. Data Nucl. Data Tables **36**, 495 (1987).
[9] A. Bohr and B. R. Mottelson, *Nuclear Structure* (W. A. Benjamin, New York, 1975), Vol. 1.
[10] I. Tanihata, H. Hamagaki, O. Hashimoto, Y. Shida, N. Yoshikawa, K. Sugimoto, O. Yamakawa, T. Kobayashi, and N. Takahashi, Phys. Rev. Lett. **55**, 2676 (1985).
[11] I. Tanihata, H. Savajols, and R. Kanungo, Prog. Part. Nucl. Phys. **68**, 215 (2013).
[12] S. Bagchi et al., Phys. Rev. Lett. **124**, 222504 (2020).
[13] M. Takechi et al., Phys. Lett. B **707**, 357 (2012).
[14] M. Takechi et al., Phys. Rev. C **90**, 061305(R) (2014).
[15] H. Nakada, Nucl. Phys. A **808**, 47 (2008).
[16] S.-G. Zhou, J. Meng, P. Ring, and E.-G. Zhao, Phys. Rev. C **82**, 011301(R) (2010).
[17] L. Li, J. Meng, P. Ring, E.-G. Zhao, and S.-G. Zhou, Phys. Rev. C **85**, 024312 (2012).
[18] Y. N. Zhang, J. C. Pei, and F. R. Xu, Phys. Rev. C **88**, 054305 (2013).
[19] H. Nakada and K. Takayama, Phys. Rev. C **98**, 011301(R) (2018).
[20] H. Kasuya and K. Yoshida, Prog. Theor. Exp. Phys. **2021**, 013D01 (2021).
[21] T. Nakamura et al., Phys. Rev. Lett. **112**, 142501 (2014).
[22] R. F. Garcia Ruiz et al., Nat. Phys. **12**, 594 (2016).
[23] M. Tanaka et al., Phys. Rev. Lett. **124**, 102501 (2020).
[24] W. Horiuchi and T. Inakura, Phys. Rev. C **101**, 061301(R) (2020).
[25] H. Nakada, Phys. Rev. C **100**, 044310 (2019).

[26] M. V. Stoitsov, J. Dobaczewski, W. Nazarewicz, S. Pittel, and D. J. Dean, Phys. Rev. C **68**, 054312 (2003).
[27] K. Minomo, T. Sumi, M. Kimura, K. Ogata, Y. R. Shimizu, and M. Yahiro, Phys. Rev. C **84**, 034602 (2011).
[28] K. Minomo, T. Sumi, M. Kimura, K. Ogata, Y. R. Shimizu, and M. Yahiro, Phys. Rev. Lett. **108**, 052503 (2012).
[29] T. Sumi, K. Minomo, S. Tagami, M. Kimura, T. Matsumoto, K. Ogata, Y. R. Shimizu, and M. Yahiro, Phys. Rev. C **85**, 064613 (2012).
[30] W. Horiuchi, T. Inakura, T. Nakatsukasa, and Y. Suzuki, Phys. Rev. C **86**, 024614 (2012).
[31] S. Watanabe et al., Phys. Rev. C **89**, 044610 (2014).
[32] T. Inakura, H. Imagawa, Y. Hashimoto, S. Mizutori, M. Yamagami, and K. Matsuyanagi, Nucl. Phys. A **768**, 61 (2006).
[33] D. Vautherin and D. M. Brink, Phys. Rev. C **5**, 626 (1972).
[34] K. T. R. Davies, H. Flocard, S. Krieger, and M. S. Weiss, Nucl. Phys. A **342**, 111 (1980).
[35] H. Flocard, S. E. Koonin, and M. S. Weiss, Phys. Rev. C **17**, 1682 (1978).
[36] J. Bartel, P. Quentin, M. Brack, C. Guet, and H. Håkansson, Nucl. Phys. A **386**, 79 (1982).
[37] E. Chabanat, P. Bonche, P. Haensel, J. Mayer, and R. Schaeffer, Nucl. Phys. A **627**, 710 (1997).
[38] P.-G. Reinhard and H. Flocard, Nucl. Phys. A **584**, 467 (1995).
[39] M. Beiner, H. Flocard, N. V. Giai, and P. Quentin, Nucl. Phys. A **238**, 29 (1975).
[40] J.-P. Delaroche, M. Girod, J. Libert, H. Goutte, S. Hilaire, S. Péru, N. Pillet, and G. F. Bertsch, Phys. Rev. C **81**, 014303 (2010).
[41] S. A. Changizi and C. Qi, Phys. Rev. C **91**, 024305 (2015).
[42] W. Horiuchi, S. Hatakeyama, S. Ebata, and Y. Suzuki, Phys. Rev. C **93**, 044611 (2016).
[43] W. Horiuchi, S. Ebata, and K. Iida, Phys. Rev. C **96**, 035804 (2017).
[44] W. Horiuchi, T. Inakura, T. Nakatsukasa, and Y. Suzuki, JPS Conf. Proc. **6**, 030079 (2015).
[45] S. G. Nilsson, Mat. Fys. Medd. Dan. Vid. Selsk. **29**, 1 (1955).
[46] X. Campi, H. Flocard, A. K. Kerman, and S. Koonin, Nucl. Phys. A **251**, 193 (1975).
[47] C. Thibault, R. Klapisch, C. Rigaud, A. M. Poskanzer, R. Prieels, L. Lessard, and W. Reisdorf, Phys. Rev. C **12**, 644 (1975).
[48] S. Nummela et al., Phys. Rev. C **64**, 054313 (2001).
[49] P. Doornenbal et al., Phys. Rev. Lett. **103**, 032501 (2009).
[50] K. Kumar, Phys. Rev. C **1**, 369 (1970).
[51] N. Tajima and N. Suzuki, Phys. Rev. C **64**, 037301 (2001).
[52] I. Hamamoto and B. R. Mottelson, Phys. Rev. C **79**, 034317 (2009).
[53] V. Choudhary, W. Horiuchi, M. Kimura, and R. Chatterjee, Phys. Rev. C **102**, 034619 (2020).
[54] K. Yoshida and N. Hinohara, Phys. Rev. C **83**, 061302(R) (2011).
[55] K. Tsukada et al., Phys. Rev. Lett. **118**, 262501 (2017).